20 November 1998

ELSEVIER

Chemical Physics Letters 297 (1998) 23–28

CHEMICAL PHYSICS LETTERS

Measuring the true helicity of carbon nanotubes

Lu-Chang Qin *

Argonne National Laboratory, Materials Science Division, 9700 South Cass Avenue, Argonne, IL 60439, USA

Received 9 March 1998; in final form 29 September 1998

Abstract

Electron diffraction patterns from carbon nanotubes have been analyzed for measuring the true helicity of carbon nanotubes. The cylindrical curvature of the tubules causes a large difference between the apparent half twist angle which appears in electron diffraction patterns and the true helical angle of the examined tubule. A direct method has been developed to calculate the cylindrical correction factors, which are vital for accurate deduction of the true helicity from electron diffraction patterns. By combining with measured diameters from real-space images, it is now possible to determine the atomic structure of carbon nanotubes.

1. Introduction

Carbon nanotubes [1] have been demonstrated to possess extraordinary physical properties by both theoretical calculations and experimental measurements. Their properties are highly structure-sensitive. Apart from the nanometer-sized diameter, a unique structural characteristic of both multiwalled [1] and single-walled [2,3] nanotubes is that they are usually helical, as indicated by their respective electron diffraction patterns. The helicity of a nanotube has important consequences in affecting the tubule properties. For example, a given single-walled carbon nanotube, depending on its diameter and helicity, can behave either as a metal or semiconductor [4,5]; chiral current has been predicted to exist in B–C–N compound nanotubes by theoretical analysis [6] and the current vectors are determined by the helicities of the tubules. For an ideal single-walled carbon nanotube, three parameters are needed to define its atomic structure completely when it is helical: diameter, helicity, and handedness. The measurement of diameter from high-resolution electron micrographs can be quite accurate when the magnification is well calibrated and if the tubule diameter is not near its lower limit of ~ 0.7 nm. Given the structural sensitivity of tubule properties, measuring the helicity of carbon nanotubes is therefore of great importance to better understand structure–property and structure–processing relationships. As the techniques for nanotube synthesis are aimed at the ultimate goal of fabricating nanotubes of designed structures, a reliable and accurate method to determine the helicities is needed. However, practical advancement in accurate measurement of tubule helicities has been slow due primarily to a lack of good working procedures and formidable experimental difficulties.

Electron diffraction has been an effective means to reveal the helical nature of nanotube structures. For a single-walled carbon nanotube lying perpendicular to the incident electron beam, the electron

* Present address: IBM, Department MXQ/014, 5600 Cottle Road, San Jose, CA 95193, USA. E-mail: qin@ibm.net

0009-2614/98/$ - see front matter
PII: S0009-2614(98)01122-1

beam passes through two graphitic layers, which are referred to as the 'top' and 'bottom' layer, respectively. When the tubule is helical, the top and bottom graphene layers are misaligned with respect to each other by a twist angle equal to twice the helical angle α. This relative twist causes the resulting graphitic electron diffraction pattern to split into two distinctive sets with a splitting angle 2θ that is most easily visible along the tubule axis. A popular method that has been widely employed to obtain helical angles neglects the cylindricality of the nanotubes. Under this assumption, the apparent half twist angle θ observed in the electron diffraction pattern is approximated as the true helical angle α of the tubule.

An early analysis of the diffraction phenomena from cylindrical tubules has led to analytic formulas for calculating the electron or X-ray diffraction amplitudes from tubules of given structure [7], in which the cylindrical curvature of nanotubes had been fully taken into account. A further development of this theory for applications to the reverse problem, i.e., to obtain the helical angles from experimental electron diffraction patterns, found that large errors often result if the cylindricality factor is not corrected [8]. The difference between the apparent half twist angle θ measured from an experimental electron diffraction pattern and the true helical angle α of the diffracting tubule can be as large as 70–80%. Fortunately, the difference can be well related by a specific order of Bessel function that expresses the cylindrical effect. Although the cylindrical correction factors have been worked out [8], the complexity of the expression makes it difficult to deduce the order of the associated dominating Bessel function with trial-and-error methods. The lack of an explicit formula has therefore made the procedure difficult to apply to routine determination of the helicities of nanotubes from experimental diffraction data.

In this Letter, simplified and straightforward analytic results are presented for calculating the order of the modifying Bessel function and therefore the cylindrical correction factors. The correction factors are graphed and are shown to be related directly to a Bessel function of specific order, which can be determined from the tubule indices $[u_1, v_1]$ that specify the perimeter of the cylindrical tubule on the graphene net. A few practical examples of single-walled carbon nanotubes with indices [12, 1], [18, 2], and [31, 13] are given as illustrations of the procedure.

2. Theoretical consideration

The atomic structure of a single-walled carbon nanotube can be described by two integer indices $[u_1, v_1]$, that specify the perimeter of the tubule in radial projection on a graphene net. The basis vectors, $\boldsymbol{a}_1$ and $\boldsymbol{a}_2$ ($a_1 = a_2 = a = 0.2451$ nm), are chosen following the crystallographic convention [9] as shown in Fig. 1a. Other choices of basis vectors

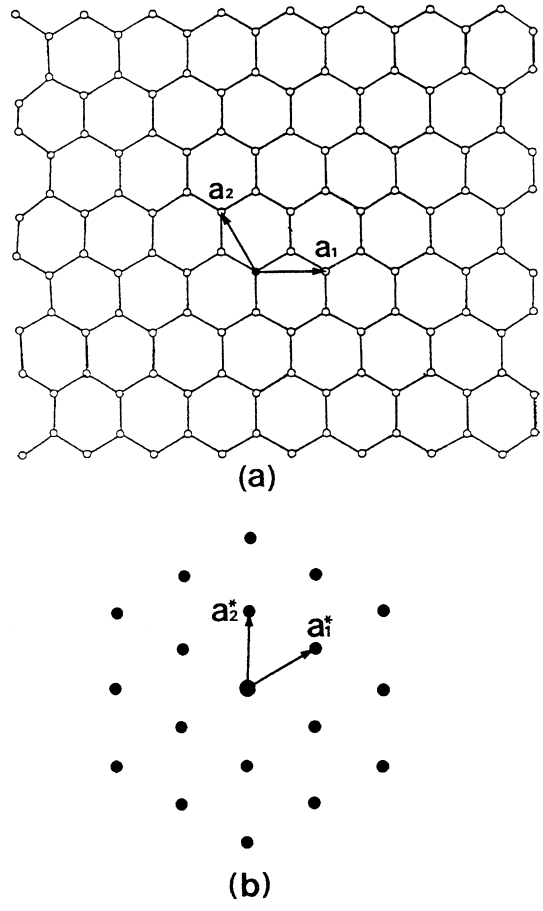

Fig. 1. (a) Structure of graphene with basis vectors $\boldsymbol{a}_1$ and $\boldsymbol{a}_2$ ($a_1 = a_2 = a = 0.2451$ nm) defined and (b) corresponding reciprocal space structure with basis vectors $\boldsymbol{a}_1^*$ and $\boldsymbol{a}_2^*$. The relative orientation between these two structures are fixed when the graphene is rotated.

should lead to equivalent physical results, though the indices may appear to be different. Once the basis vectors are chosen, other structural parameters, such as tubule perimeter $\boldsymbol{A}=[u_1, v_1]$ (or diameter $d=A/\pi$), helical angle α, and tubule axis $\boldsymbol{B}=[u_2, v_2]$, etc., can be deduced from these two indices:

$$A = a\left(u_1^2 + v_1^2 - u_1 v_1\right)^{1/2}, \tag{1}$$

$$u_2/v_2 = (u_1 - 2v_1)/(2u_1 - v_1), \tag{2}$$

$$\alpha = \cos^{-1}\left[(2u_1 - v_1)/2\left(u_1^2 + v_1^2 - u_1 v_1\right)^{1/2}\right]. \tag{3}$$

It should be noted that the indices u_2 and v_2 should be chosen in such a way that there should be no other common factors except unity.

For a general case, i.e., with atoms positioned at discrete locations (r_0, ϕ_j, z_j) on a helix of radius r_0, the corresponding structure factor F in polar coordinates (R, Φ, l) can be expressed in the following form [7]:

$$F(R, \Phi, l) = \sum_n \exp\left[\mathrm{i}n(\Phi + \pi/2)\right] J_n(2\pi r_0 R) \times \sum_j f_j \exp\left[\mathrm{i}\left(n\phi_j + 2\pi l z_j/B\right)\right], \tag{4}$$

where f_j is the atomic scattering amplitude for atom j, $J_n(u)$ is the Bessel function of order n, B is the periodicity of the structure along the z-direction (tubule axis), the summation for j is done over all atoms in an asymmetric cell, and n is summed over all integers as allowed by the selection rule determined by the structure [7].

When the above Eq. (4) is rewritten as

$$F(R, \Phi, l) = \sum_n B_n(R, \Phi) T_{nl}, \tag{5}$$

with

$$B_n(R, \Phi) = \exp\left[\mathrm{i}n(\Phi + \pi/2)\right] J_n(2\pi r_0 R) \tag{6}$$

and

$$T_{nl} = \sum_j f_j \exp\left[2\pi\mathrm{i}\left(nx_j/A + lz_j/B\right)\right], \tag{7}$$

where (x_j, z_j) are the Cartesian coordinates of atom j in radial projection, the diffraction from a cylindrical tubule is more clearly seen by dividing the pattern into two parts: (a) the structure factor in radial projection described by T_{nl}; and (b) the modifying function $B_n(R, \Phi)$ taking into account of the effect of cylindrical curvature. For the case of single-walled carbon nanotubes, T_{nl} gives rise to the regular hexagonal diffraction pattern from graphene as shown in Fig. 1b. As indicated by Eq. (5), the modifying Bessel function alters the intensity peak positions in the diffraction pattern, and the shifts are determined by the order of the acting Bessel function. As shown in [8], the shift for $n=1$ is $\sim 80\%$, and the shift for $n=2$ is $\sim 50\%$, etc. In general, the cylindrical correction factor for a given order of Bessel function $J_n(2\pi r_0 R)$ is expressed by the following equation [8]:

$$\tan(\theta) = (u_n/n)\tan(\alpha), \tag{8}$$

where θ is the apparent half twist angle measured from an experimental electron diffraction pattern, α is the true helical angle of the tubule, and u_n is the value of u at which the Bessel function $J_n(u)$ assumes its first maximum for $n \neq 0$. The correction factors are plotted for various low values of n in Fig. 2.

For a given tubule structure $[u_1, v_2]$, when the graphene structure is indexed as illustrated in Fig. 1, the apparent twist angle can be measured most conveniently on either (100) type (for helical angles $0° \leq \alpha \leq 15°$) or (110) type (for helical angles $15° \leq \alpha \leq 30°$) reflections. Given the very weak effect due

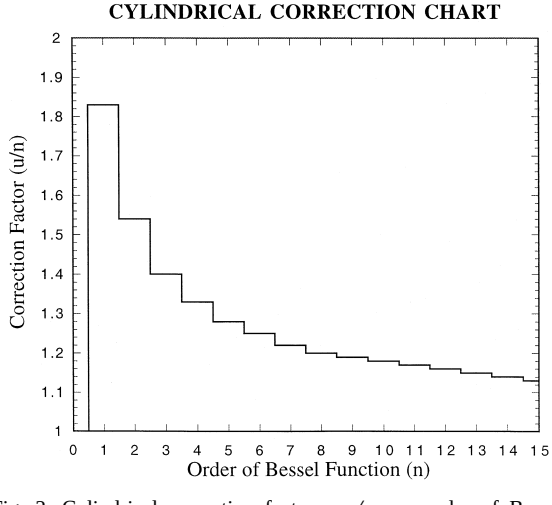

Fig. 2. Cylindrical correction factor u_n/n vs. order of Bessel function n. The correction factor is large for low values of n. For example, when $n=1$, the correction factor is $\sim 80\%$.

to the discontinuity of the scattering Coulombic potential [7], the selection rule should therefore be such that the reflection $\boldsymbol{G}$ from the radial projection net should fall onto the reciprocal lattice point $\boldsymbol{g}$ of the graphene structure. Let $\boldsymbol{A}^*$ and $\boldsymbol{B}^*$ ($A^* = 1/A$; $B^* = 1/B$) be the basis vectors of the reciprocal lattice of the radial projection net of the tubule, the selection rule is then

$$\boldsymbol{G} = \boldsymbol{g}\,, \tag{9}$$

or equivalently

$$n\boldsymbol{A}^* + l\boldsymbol{B}^* = h\boldsymbol{a}_1^* + k\boldsymbol{a}_2^*\,, \tag{10}$$

for the general case where

$$\boldsymbol{G} = n\boldsymbol{A}^* + l\boldsymbol{B}^* \tag{11}$$

and

$$\boldsymbol{g} = h\boldsymbol{a}_1^* + k\boldsymbol{a}_2^*\,. \tag{12}$$

Noting that

$$lB^* = g\sin(\gamma - \alpha)\,, \tag{13}$$

as illustrated in Fig. 3a, where γ is the angle between the chosen reflection $\boldsymbol{g}$ and basis vector $\boldsymbol{a}_1$, then the selection rule $\boldsymbol{G} = \boldsymbol{g}$ can be further simplified to the following form:

$$n = hu_1 + kv_1\,. \tag{14}$$

This result is valid for the general geometry where the helical angle is measured clockwise with respect to the horizontal axis that is perpendicular to the tubule axis as shown in Fig. 3. Two specific sets of reflections are worthy of special attention: (100) and (110) and their respective crystallographic equivalents on which the measurement of twist angles 2θ is usually performed. For reflection (010) [its crystallographically equivalent reflections are $(1,0,0)$, $(1,-1,0)$, $(0,-1,0)$, $(-1,0,0)$, and $(-1,1,0)$], $\boldsymbol{g} = \boldsymbol{a}_2^*$, as schematically illustrated in Fig. 3b, the selection rule is determined by equation

$$n = v_1\,. \tag{15}$$

While for reflection $(-1,2,0)$ [its crystallographically equivalent reflections are $(1,1,0)$, $(-2,1,0)$, $(-1,-1,0)$, $(1,-2,0)$ and $(2,-1,0)$], as illustrated in Fig. 3c, where $\boldsymbol{g} = -\boldsymbol{a}_1^* + 2\boldsymbol{a}_2^*$, the selection equation corresponding to Eq. (15) is

$$n = -u_1 + 2v_1\,. \tag{16}$$

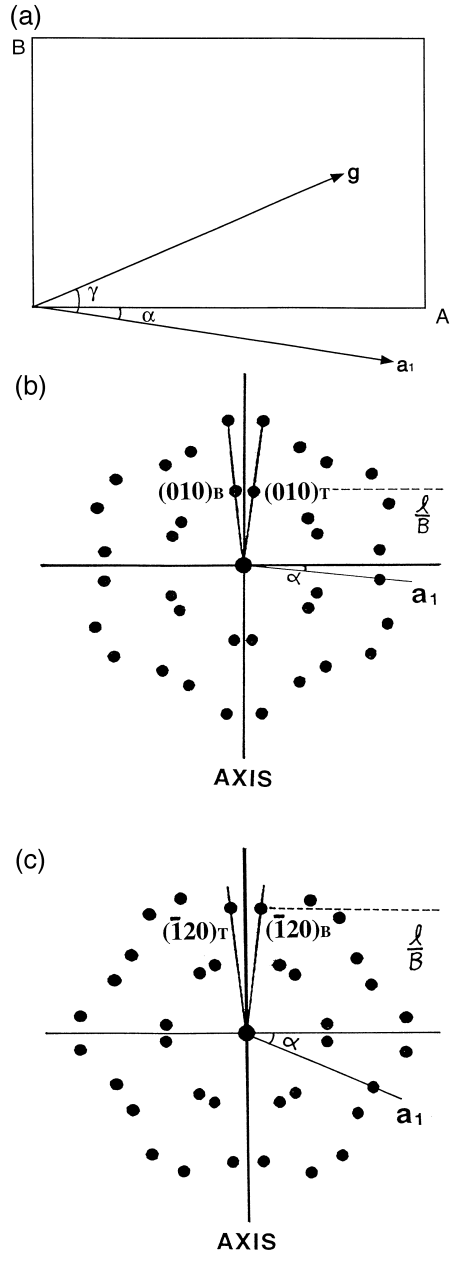

Fig. 3. (a) Geometric relationship between the primary graphene reflections $\boldsymbol{g}$ within the framework of radially projected unit cell of length A and height B. (b, c) Schematic diffraction patterns from single-walled carbon nanotubes for the measurement of twist angles for (b) near-zigzag structure and (c) near-armchair structure, respectively. Subscripts T and B refer to the top and bottom layer of the tubule, respectively.

Eqs. (15) and (16) restrict the helical angles within the range $[0°, 30°]$. The above equations can also make the calculation of electron diffraction patterns of carbon nanotubes fast and straightforward.

3. Results and discussion

For tubule $[u_1, v_1] = [12, 1]$, the helical angle is $\alpha = 4.3°$. Using Eq. (15), when the apparent half twist angle is measured on the (010) reflection, the modifying Bessel function should have the order $n = 1$. Therefore the measured apparent half twist angle θ would be enlarged by $\sim 80\%$ to become 7.5°, as shown by Eq. (8). This is confirmed by numerical calculations using Eq. (4) as shown in Fig. 4a, where the apparent twist angle 2θ between the two (010) reflections (T and B designate the top and bottom layer of the tubule, respectively) is measured to be $\sim 15°$. It is interesting to note that, for the (020) reflection, the modifying Bessel function has the order of 2, so the apparent half twist angle θ becomes accordingly smaller, which is actually measured to be $\sim 6.5°$ (50% difference), as indicated in the correction chart (Fig. 2). Fig. 4b shows the case for tubule $[18, 2]$, where $\alpha = 5.8°$ and $\theta = 9°$ with $n = 2$.

The above two examples have helical angles $0° \leq \alpha \leq 15°$, so the (010) reciprocal lattice vector lies nearly parallel to the tubule axis (off-axis angle α, see Fig. 3b). On the other hand, for the tubule $[u_1, v_1] = [31, 13]$, its helical angle is $\alpha = 24.7°$. In this case, the (110) reflections should be nearly parallel to the tubule axis $[u_2, v_2] = [5, 49]$. The apparent half twist angle measured from the simulated electron diffraction pattern is 7° (Fig. 4c), which is $\sim 30\%$ large than the twist angle with respect to the tubule axis $(30° - \alpha)$. Using Eq. (16), the acting Bessel function should be of order $n = 5$, which gives rise the correction factor $\sim 30\%$, as shown in the correction chart (Fig. 2). The experimental electron diffraction patterns from all the above-indexed single-walled carbon nanotubes can be found in literature [8].

An interesting effect is that even when the order of Bessel functions becomes large, the cylindrical correction factors are still not negligible. For example, for $n = 20$ and $n = 40$, the cylindrical correction

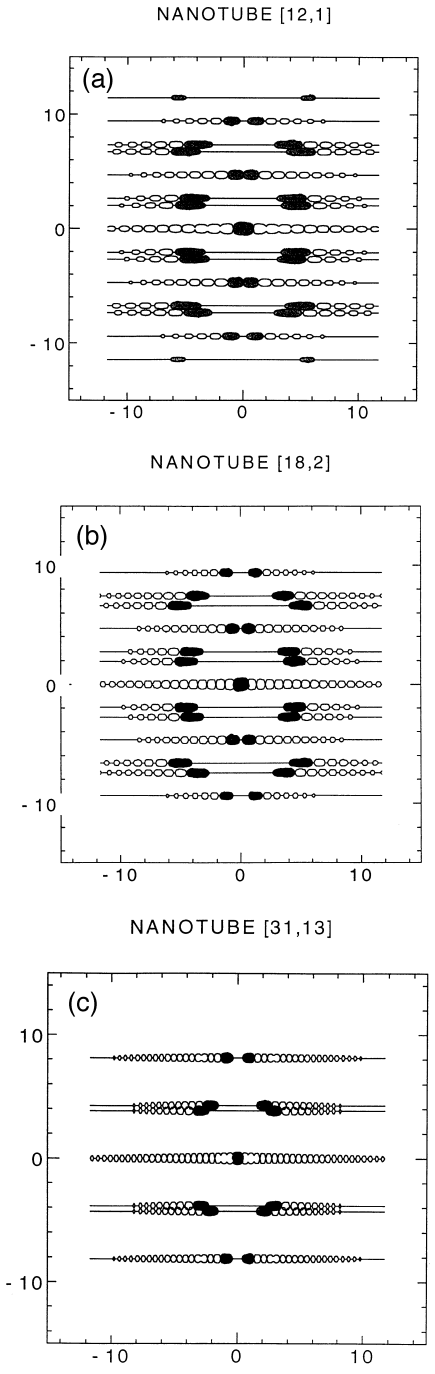

Fig. 4. Calculated electron diffraction intensity distribution for carbon nanotubes: (a) [12, 1] ($d = 0.90$ nm, $\alpha = 4.3°$); (b) [18, 2] ($d = 1.33$ nm, $\alpha = 5.8°$); and (c) [31, 13] ($d = 2.10$ nm, $\alpha = 24.7°$).

factors are still ~ 1.11 and ~ 1.07, respectively. This fact results in a lateral stretching of the hexagonal Fraunhofer diffraction pattern by $\sim 10\%$. This effect is observable in both simulated and experimental diffraction patterns [12].

Though the method presented here has been limited to dealing with single-walled carbon nanotubes, the principles and algorithms are valid for multi-walled carbon nanotubes or cylindrical tubules formed by other types of atoms. The extension to these cases is straightforward.

It should be noted that the electron diffraction patterns possess 2mm symmetry. This is true even when the tubule is tilted away from directions perpendicular to the incident electron beam, though the projected structure along the electron beam direction may not necessarily have 2mm symmetry.

The procedure proposed here should allow easy measurement of the true helicity of carbon nanotubes. For example, in laser evaporation, individual and raft-like bundles of single-walled carbon nanotubes [10–13] are produced. Although substantial attempts have been made to correlate the processing parameters with tubule diameters, it is still far from being conclusive in correlating the processing conditions and tubule helicities. With regard to the property–structure relationship, one example is the sensitivity of electric-field induced electron emission from carbon nanotubes. With manipulatable nanotubes available [14], it is expected that the property–structure relationship, in particular the property–diameter–helicity relationship will be better understood in the near future.

4. Conclusions

The true helicity α of a carbon nanotube $[u_1, v_1]$ can be deduced from the half twist angle θ measured on an experimental electron diffraction pattern. The cylindrical correction factor due to the curvature of the measured tubule is determined by a Bessel function of order n, which can be calculated directly from the tubule indices

(a) $n = v_1$, for $0° \leq \alpha \leq 15°$;

(b) $n = u_1 - 2v_1$, for $15° \leq \alpha \leq 30°$.

Without the correction, the resulted error can be as large as 80%, depending on the order of the modifying Bessel functions.

Acknowledgements

The author wishes to thank Dr. M.A. Kirk for his encouragement. This work is partially supported by the United States Department of Energy Office of Basic Energy Sciences under Contract W31-109-ENG-38.

References

[1] S. Iijima, Nature (London) 354 (1991) 56.
[2] S. Iijima, T. Ichihashi, Nature (London) 363 (1993) 603.
[3] D.S. Bethune, C.-H. Kiang, M.S. de Vries, G. Gorman, R. Savay, J. Vazquez, R. Beyers, Nature (London) 363 (1993) 605.
[4] H. Hamada, S. Sawada, A. Oshiyama, Phys. Rev. Lett. 68 (1992) 1579.
[5] R. Saito, M. Fujita, G. Dresselhaus, M.S. Dresselhaus, Phys. Rev. B 46 (1992) 1804.
[6] Y. Miyamoto, S.G. Louie, M.L. Cohen, Phys. Rev. Lett. 76 (1996) 2121.
[7] L.C. Qin, J. Mater. Res. 9 (1994) 2450.
[8] L.C. Qin, T. Ichihashi, S. Iijima, Ultramicroscopy 67 (1997) 181.
[9] T. Hahn (Ed.), International Tables for Crystallography, vol. A, 3rd ed., Kluwer, Dordrecht, 1992.
[10] A. Thess, R. Lee, P. Nikolaev, H. Dai, P. Petit, J. Robert, C. Xu, Y.H. Lee, S.G. Kim, A.G. Rinzler, D.T. Colbert, G.E. Scuseria, D. Tomanek, J.E. Fisher, R.E. Smalley, Science 273 (1996) 483.
[11] L.C. Qin, S. Iijima, Chem. Phys. Lett. 269 (1997) 65.
[12] L.C. Qin, S. Iijima, H. Kitaura, Y. Maniwa, S. Suzuki, Y. Achiba, Chem. Phys. Lett. 268 (1997) 101.
[13] J.M. Cowley, P. Nikolaev, A. Thess, R.E. Smalley, Chem. Phys. Lett. 265 (1997) 379.
[14] L.C. Qin, S. Iijima, Mater. Lett. 30 (1997) 311.